ESTIMATION OF STIMULUS ATTENUATION IN COCHLEAR IMPLANTS

Jacoba E. Smit[*], Tania Hanekom and Johan J. Hanekom

Department of Electrical, Electronic and Computer Engineering, University of Pretoria, Lynnwood Road, Pretoria, 0002, South Africa

Type of paper: Reseach article

Total number of

(i) pages 52 (including title page)

(ii) figures 6

(iii) tables 6

[*] *At the time of this research JE Smit was with the University of Pretoria and now resides at the Biophotonics group, National Laser Centre (NLC), CSIR, P.O. Box 395, Pretoria, 0001, South Africa*

Abstract (174 words)

Neural excitation profile widths at the neural level, for monopolar stimulation with Nucleus straight and contour arrays respectively, were simulated using a combined volume conduction-neural model. The electrically evoked compound action potential profile widths at the electrode array level were calculated with a simple approximation method employing stimulus attenuation inside the cochlear duct, and the results compared to profile width data from literature. The objective of the article is to develop a simple method to estimate stimulus attenuation values by calculating the values that best fit the modelled excitation profile widths to the measured evoked compound action potential profile widths. Results indicate that the modelled excitation profile widths decrease with increasing stimulus attenuation. However, fitting of modelled excitation profile widths to measured evoked compound action potential profile widths show that different stimulus attenuation values are needed for different stimulation levels. It is suggested that the proposed simple model can provide an estimate of stimulus attenuation by calculating the value of the parameter that produces the best fit to experimental data in specific human subjects.

Keywords stimulus attenuation, length constant, computational model, evoked compound action potential, neural excitation spread, human auditory nerve fibre

INTRODUCTION

Cochlear implants have been developed to help rehabilitate profoundly deaf persons by providing them with a measure of sound perception through electrical stimulation of auditory nerve fibres (ANFs). However, while the average performance of cochlear implants has improved over the last three decades, large variability in speech performance across individual implant users is still a major problem (Shannon et al., 2004). This can in part be ascribed to dissimilar neural excitation spread patterns, both intrasubject and intersubject, as a result of variability in factors such as implant type, degree of degeneration of the auditory nerve fibre population across human subjects, electrode geometry, intrascalar electrode location and stimulation strategy (Nadol Jr, 1990; Schuknecht, 1993; Zimmermann et al., 1995; Nadol Jr, 1997; Cohen et al., 2003; Arts et al., 2003; Abbas et al., 2004; van Wieringen et al., 2005; Fayad and Linthicum Jr, 2006). Even though potential implantees undergo pre-operative auditory testing, the successful outcome of the implantation is not known until after the implant has been switched on (Niparko, 2004). Ideally the electrodes should be situated closest to the sites of surviving ANFs, since this leads to reduced power consumption in the implant, lower stimulation thresholds, narrower neural excitation spread patterns and an increased dynamic range (Townshend and White, 1987; Shepherd et al., 1993; Rebscher et al., 2001; Abbas et al., 2004; Leake and Rebscher, 2004; Glueckert et al., 2005). Middlebrooks and Snyder (2007; 2008) proposed lowering of thresholds through intramodiolar placement of an electrode array, but this type of electrode placement is currently not in use in human implantees. A telemetric measuring system for cochlear implants, called Neural Response Telemetry (NRT) by Cochlear Limited, is available to measure the electrically evoked compound action potential (ECAP) of the ANFs (see for example Abbas et al., 1999; and Dillier et al., 2002). ECAP data can be used to obtain an

objective estimate of the dynamic range, and possibly give a hint as to the extent of neural survival (see for example Abbas et al., 1999; Franck and Norton, 2001; and Dillier et al., 2002). It is also used to examine the extent to which psychophysical measurements reflect the amount of neural excitation spread (Cohen et al., 2003).

ECAP data are obtained by a forward masking paradigm and it is generally assumed that psychophysical forward masking profiles provide an indirect measure of neural excitation patterns (van der Heijden and Kohlrausch, 1994; Chatterjee and Shannon, 1998; Abbas et al., 2004). In the case of ECAP data, the measure is more proximal to the peripheral neural activity than for psychophysical forward masking, since it is assumed that the central auditory processes do not contribute to the masking profile. Furthermore, the amplitude measurement of the ECAP gives an indication of the number of responding fibres (Miller et al., 1999). Cohen et al. (2003) reported that larger ECAP profile widths are measured in implantees with higher MCLs, indicating a wider spread of neural excitation. The spread in excitation also increases with an increase in stimulus level (Abbas et al., 2004). Miller et al. (2003) used the fact that the ECAP reflects the gross ensemble response of a neural population to investigate the effects of stimulation mode on neural excitation spread in cats. The results indicate that monopolar stimulation produces wider ECAP profiles than bipolar stimulation, consistent with the observation that monopolar stimulation causes wider neural excitation (van den Honert and Stypulkowski, 1987). Studies performed on human subjects, however, either support or disagree with these animal findings. Townshend and White (1987) developed a paradigm based on the psychophysical thresholds measured for two human implantees to calculate the current spread patterns around the electrodes of a modelled electrode array. Their simulations confirmed wider neural excitation spread with monopolar compared to bipolar stimulation, as well as a reduction in excitation spread for an electrode array placed

closer to the modiolus. A more recent study by Kwon and van den Honert (2006), however, suggest that the neural excitation spread of bipolar stimulation is not always consistently more focussed than for a monopolar stimulus of equal loudness. The difference in results may indicate that the assumption that the ECAP reflects the gross ensemble response of a neural population may not be entirely correct, as suggested by a modeling study of Briaire and Frijns (2005).

The development of a comprehensive model to simulate ECAPs is beyond the scope of this study. However, ECAP profile widths can be used to estimate stimulus attenuation. Stimulus attenuation (characterised by length constant) directly relates to current distribution and thus the extent of neural excitation inside the cochlea. There have been only a few studies to determine the stimulus attenuation inside the cochlea (Black and Clark, 1980; Spelman et al., 1982; Black et al., 1983; Hartmann and Klinke, 1990; Kral et al., 1998; Vanpoucke et al., 2004; Bingabr et al., 2008; Nelson et al., 2008). Most of these have been reported for *in vivo* and *in vitro* measurements on cat, with length constants ranging between 3 – 16 mm for monopolar intracochlear stimulation (Black and Clark, 1980; Black et al., 1983; Hartmann and Klinke, 1990; Kral et al., 1998). Nelson et al. (2008) obtained a length constant of 6.0 mm for monopolar stimulation in human, while Bingabr et al. (2008) predicted monopolar current decay of about 2 mm length constant with an acoustic vocoder model.

The present study focuses on the influence of the variation in the stimulus attenuation on neural excitation spread for monopolar stimulation of an electrode located in the basal part of the human cochlea. A simple method was developed to estimate ECAP profile widths as a function of stimulus attenuation parameter. The objective of the paper is to predict with this method the values of the stimulus attenuation that best map the modelled ECAP profile

widths to the measured ECAP profile widths obtained from a study by Cohen et al. (2003). A recently developed human auditory nerve fibre (ANF) model, coupled to a volume conduction cochlear model by Hanekom (2001) was used to predict the widths of neural excitation spread as a result of specific stimuli (Smit et al., 2008; Smit, 2008). Integrity of the simple method algorithm was verified by obtaining stimulus attenuation estimates with the longer established Generalised Schwarz-Eikhof-Frijns (GSEF) auditory nerve fibre model developed by Frijns et al. (2000).

MATERIALS AND METHODS

1. Models of the implanted cochlea and auditory nerve fibre

1.1 The volume conduction cochlear model

Simulations were performed using the resistances from a 3D spiralling finite element volume-conduction model of the first one-and-a-half turns of the electrically stimulated human cochlea, coupled to a auditory nerve fibre (ANF) model (Figs. 1, 3(a) and 3(b)). For more details on the volume conduction model refer to Hanekom (2001). The amplitudes of stimulation pulses at the nerve fibres were derived from the external potential distribution, which was in turn calculated from the Ohmic resistances from the volume-conduction model.

---------- *Suggested position of Figure 1* ----------

The modelled cochlea was stimulated with a monopolar electrode configuration, with the stimulated electrode located in the basal cochlear turn and the return electrode lying outside

the cochlea. The pulsatile stimulus waveform was a biphasic, charge-balanced, square pulse without interphase gap, with equal cathodic and anodic phases of 40 μs duration. Only single-pulse responses were calculated.

Simulations were performed for two electrode array positions, one lateral (Nucleus 24 straight array) and one medial (Nucleus 24 contour array), relative to the modiolus (Cohen et al., 2003; Miller et al., 2004). The straight array was modelled with full-band electrodes and the contour array with half-band electrodes (Abbas et al., 2004; Miller et al., 2004)

1.2 The human auditory nerve fibre model

The Type I human ANF model was based on the ANF cable model by Rattay et al. (2001), but with the axon replaced with a recently developed generalised human sensory nerve fibre model (Smit, 2008). The nerve fibre morphology is shown in Fig. 2. An additional modification to the ANF model was a shortening of the dendrite to fit the somal position of its counterpart in the volume conduction cochlear model. Details of the human ANF model are provided in Appendix A.

---------- *Suggested position of Figure 2* ----------

1.3 The generalised Schwarz-Eikhof-Frijns nerve fibre model

Frijns et al. (1994; 1995; 2000) developed a model based on the Schwarz-Eikhof nerve fibre model for rat (Schwarz and Eikhof, 1987), but adapted with guinea-pig morphometry. Recently this Generalised Schwarz-Eikhof-Frijns (GSEF) model was adapted for human ANF

simulations by employing human morphometric data only (Briaire and Frijns, 2005; Briaire and Frijns, 2006). This model, however, cannot fully account for the ECAP morphology observed in humans. To facilitate comparison of the differences between an animal and human nerve fibre models, the former guinea-pig version was employed in this study.

1.4 Modelling the degenerate nerve fibre

The degeneration and subsequent loss of ANFs resulting in hearing loss can be classified as primary or secondary. Primary neural degeneration is the normal age-related hearing loss a person experiences, while secondary (retrograde) neural degeneration is due to various factors including ototoxic substances, disease or trauma to the cochlear structures (Nadol Jr, 1990; Schuknecht, 1993). Retrograde neural degeneration, in which the dendrites retract but the somas and axons survive, occurs in persons with profound sensory hearing loss, and concerns mostly Type I ANFs (Spoendlin and Schrott, 1989; Nadol Jr, 1990; Schuknecht, 1993; Fayad and Linthicum Jr, 2006).

Since not all ANFs are affected by retrograde degeneration, simulations were performed with two versions of the nerve fibre models, simulating the effects of non-degenerated and increasingly degenerated nerve fibres respectively. Degenerated versions of the nerve fibre models were used to simulate the effect of neural degeneration, i.e. to simulate a nerve fibre with almost no peripheral (dendritic) process. This was effected by removing the first four nodal and internodal sections in the case of the modelled human ANF (refer to Fig. 1) and the first four internodal sections in the case of the GSEF model respectively. This was similar to the method employed by Frijns et al. (1996) and Briaire and Frijns (2006). The first node in the degenerated versions thus corresponded to node $\boldsymbol{n_5}$ in Fig. 2.

2. ECAP profile widths at the electrode array level

The output of the ANF model is a neural excitation profile (Fig. 3(c)), at the location of the ANFs (subsequently called neural level), showing the stimulus intensity at which an ANF at a specific location along the length of the basilar membrane will be excited. To compare the predicted excitation widths and NRT results, the excitation widths, i.e. the ECAP profile widths, at the location of the stimulating electrode array (subsequently called electrode array level) need to be determined. Ideally, this will be done by solving the inverse problem (for details see Briaire and Frijns, 2005, where the authors refer to this as the backward problem).

To facilitate estimation of the stimulus attenuation factor, a simple approximation to solving the inverse problem is used. The data of Cohen et al. (2003) provide ECAP response widths at various loudness levels, specified as percentages of the MCL. The position of the modelled probe electrode corresponded to Cohen et al.'s electrode 6 (i.e. a basal position). To model ECAP profile widths, the measured dynamic range data for electrode 6 of each of the seven Cohen et al. subjects were mapped onto the estimated neural excitation profiles calculated with the nerve fibre model. Mapping was performed by translating the dynamic range data to decibel values above threshold (defined at zero decibel) corresponding to the 20%, 50% and 80% loudness levels for each subject. The estimated widths of the ECAP response at the neural level at these loudness levels were then read from the modelled neural excitation profiles (Fig. 3(c)).

---------- *Suggested position of Figure 3* ----------

A dimensionless, normalized potential step (value = 1 for activated nerve fibres, and zero elsewhere) was generated for each of these widths (Fig. 3(d)) and used as the source in the calculation of potential field distributions at the electrode array level (Fig. 3(e)). To perform these calculations, three simplifications with regard to real cochleae were made. First, an isotropic medium was assumed in the space between the neural and electrode array levels, although an anisotropic medium was assumed in the volume-conduction cochlear model. Second, constant distances were assumed between the neural level and each of the respective electrode array levels. Values for these distances were sourced from the volume-conduction model. Third, a transverse exponential decay of voltage inside the scala tympani was assumed (Black and Clark, 1980; O'Leary et al., 1985; Bingabr et al., 2008). Using an estimated value for the stimulus attenuation, each potential field distribution at the electrode array level was derived as the summation of the potential field contributions of all the activated ANFs as specified by the individual step functions. The full width half maximum (FWHM) of each distribution, i.e. the width of the potential distribution at 50% of its peak amplitude, determined the excitation widths, similar to the technique used by Cohen et al. (2003).

RESULTS

1. Neural excitation profiles

Neural excitation profiles were calculated with the ANF model (Figs. 4(a) and (b)). For contour array stimulation profiles for degenerate nerve fibres predicted wider profiles, compared to straight array stimulation where the non-degenerate and degenerate nerve fibre

populations predicted similar profile widths. Neural excitation profile widths were determined as discussed in the Materials and Methods section.

Neural excitation profile widths were also calculated with the Generalised Schwarz-Eikof-Frijns (GSEF) model by Frijns et al. (1994; 1995; 2000) in combination with the same volume-conduction model used in this study (Figs. 4(c) and (d)). For details refer to Hanekom (2001).

GSEF model neural excitation profiles differed from those of the ANF model. In contrast to the ANF model the GSEF model predicted similar neural excitation profiles, and hence profile widths, for degenerate and non-degenerate nerve fibre populations when stimulated with the contour array. For the straight array wider neural excitation profiles are predicted for a degenerate than a non-degenerate nerve fibre population.

---------- *Suggested position of Figure 4* ----------

2. Predicted versus measured ECAP profile widths

2.1. Measured ECAP profile widths

Cohen et al. (2003) reported the widths of the ECAP profiles at FWHM at 80%, 50% and 20% loudness levels. The width ranges of seven subjects, four straight array and three contour array subjects, for probe electrode 6 are summarised in Table 1.

---------- *Suggested position of Table 1* ----------

Width data at the 20% level are available for only one subject using the straight array, and for none of the subjects using the contour array. Cohen et al. observed that the profile widths of the contour array are narrower than those of the straight array.

3.2.2. ANF model predicted ECAP profile widths

Predicted ECAP profile width results at the electrode array level for degenerate and non-degenerate ANF populations respectively, are shown in Table 2. A stimulus attenuation length constant of 1.58 mm was used in the simulations for goodness of fit to the Cohen et al. results. This value was within the range of stimulus attenuation values reported in literature (Black and Clark, 1980; Spelman et al., 1982; Black et al., 1983; Kral et al., 1998; Vanpoucke et al., 2004; Bingabr et al., 2008; Nelson et al., 2008) and was reached after consideration of the results presented in Table 3 and Figs. 5(a) and (b). The width of the distribution was taken at FWHM.

---------- *Suggested position of Table 2* ----------

The ECAP profile widths for both the straight and contour arrays followed the expected trend, i.e. to decrease with a decrease in loudness level. However, if the profile width ranges between the two arrays were compared, the difference in width at the electrode array level was smaller compared to the difference observed at the neural level. The contour array also demonstrated narrower profile width ranges than the straight array. Furthermore, the profile width values for the contour array lay closer to the lower limit of the value range for the straight array.

Comparison between the degenerate and non-degenerate cases for the straight array predicted similar width ranges, with the degenerate case slightly wider than the non-degenerate case. For the contour array the width ranges for the degenerate case were wider than for the non-degenerate case. The reason for these differences is that at the neural level, the neural excitation profiles for the degenerate and non-degenerate cases were similar, while for the contour array there was a marked difference between the two cases.

3.2.3. Normalised ECAP profile width ranges

Figs. 5(a) and (b) shows the simulated ECAP profile width ranges calculated with the ANF model, normalised to the width ranges measured by Cohen et al. Normalisation was done by dividing measured values by predicted widths. The ECAP profile widths for the straight array generally compared well for both degenerate and non-degenerate ANF cases, with the measured ranges at the 80% level reasonably centred on the predicted ranges, although the upper limits were underestimated by up to 48%. For the 50% levels the width ranges were underestimated, but were within 53% of the upper limits of the measured ranges. Cohen et al. measured the ECAP profile width for only one straight array subject at the 20% level, and the predicted value overestimated the measured valued by about 30%.

Width ranges at the 80% level were overestimated for the contour array, but the upper limits of the measured ranges were within 22% of the predicted ranges. The upper limits of the measured values at the 50% level were overestimated up to 36% by the predicted values, while the lower limits fell within 15% underestimation by the predicted values.

Normalised ECAP width ranges calculate with the GSEF model for straight and contour arrays for degenerate and non-degenerate nerve fibre populations are shown in Figs. 5(c) and (d). Normalisation was done in the same way as for Figs. 5(a) and (b). The best fit to the Cohen et al. results was for a stimulus attenuation length constant of 2.48 mm. The contour array demonstrated narrower profile width ranges than the straight array. The profile width ranges between the two arrays for the non-degenerated case were also similar, in contrast to the larger differences observed for the degenerated case (compare with Figs. 4(c) and (d)). Furthermore, the profile width values for the contour array lie closer to the upper limit of the value range for the straight array. The reasons for these differences lay in the way the two cases were modelled, with resultant similar potential step functions for the non-degenerated case resulting in similar neural response potential distributions.

---------- *Suggested position of Figure 5* ----------

---------- *Suggested position of Figure 6* ----------

3.3. Stimulus attenuation

To exemplify the effect of stimulus attenuation on ECAP profile widths, the latter (for Cohen's subject S3) are shown as a function of stimulus attenuation length constant at the electrode array level (Fig. 6). Results for the other subjects were similar and are not shown. The ECAP profile widths decreased with decreasing stimulus attenuation length constant. Since we assumed an exponential relationship between length constant and stimulus attenuation (in dB/mm), this meant that the ECAP profile widths asymptotically approached zero for large values of the stimulus attenuation (i.e. small values of the length constant).

---------- *Suggested position of Table 3* ----------

The stimulus attenuation length constant values that provided the best fit to Cohen et al.'s results are presented in Table 3. Owing to lack of information about the 20% loudness level data for the contour array, no stimulus attenuation values could be estimated. It appeared as though i) stimulus attenuation was relatively unchanged between the 50% and 80% loudness levels but increased for the 20% level and ii) that intersubject variation in stimulus attenuation existed at a specific loudness level.

DISCUSSION

Javel et al. (1987) reported lower thresholds for fibres located closer to the stimulating electrodes. Fibres located further from the stimulating electrode could only be excited at higher stimulus intensities. Miller et al. (1993) and Shepherd et al. (1993) showed large threshold changes and growth rate of the fibre's ECAP response when the location of the intracochlear stimulus electrode was changed. Modelling data by Briaire and Frijns (2006) and Hanekom (2001) also predicted a reduction in neural threshold as the stimulating electrodes were moved closer to the modiolus, with the greatest reduction for fibres lying closest to the electrodes. The modelled results for both the human ANF and GSEF models agreed with these and Cohen et al.'s (2003) findings, showing that as the loudness levels (or stimulus intensity) increased, the ECAP profile width (i.e. neural excitation spread) increased.

Simulation results showed more localised excitation spread for the contour array compared to the straight array, in both the non-degenerated and degenerated nerve fibre cases. This is

consistent with the observation that the straight array is located further away from the modiolus than the contour array. Single-fibre studies by Ranck (1975) and model results by, among others, Rattay (1990) indicate that the threshold current increases with the square of the distance from the electrode, with a resultant wider potential field distribution. This has the effect that as the fibre distance from the electrode increases, the excitation region around the electrode increases, since more Ranvier nodes will fall inside the depolarised region, causing a larger number of nerve fibres to be excited at a specific stimulus intensity relative to the threshold stimulus intensity (e.g. Shepherd et al., 1993; Cohen et al., 2001; Frijns et al., 2001; and Cohen et al., 2003).

Excitation in degenerate fibres is expected to occur more centrally along the fibre, i.e. axonal excitation, since retrograde degeneration causes the dendrites to retract, while the somas and axons survive (Spoendlin and Schrott, 1989; Nadol Jr, 1990; Schuknecht, 1993). This is confirmed by, among others, a modelling study by Frijns et al. (1996) employing the GSEF model, and more recently with their updated human version of the GSEF model (Briaire and Frijns, 2006). It can therefore be assumed that thresholds predicted for non-degenerate fibres located in close vicinity to the stimulating electrode will be lower than for degenerate fibres, owing to the spatial arrangement of fibres (refer to the cross-sectional diagram of the modelled cochlea employed in this study, as shown in Fig. 2). From Fig. 2 it is clear that each ANF is shaped in a curved fashion, with the dendrites in general located closer to the electrode array than the axons, even more so for ANFs located close to an electrode compared to ANFs located between two consecutive electrodes. Unfortunately this cannot be seen clearly from the neural excitation profiles depicted in Fig. 4, since the minima of all profiles was shifted to 0 dB to facilitate easier comparison of profile widths.

What is apparent from the profiles in Fig. 4 however are the differences in profile shape between non-degenerate and degenerate ANFs for the contour and straight arrays respectively when the human ANF (Figs. 4(a) and (b)) and GSEF (Figs. 4(c) and (d)) models are compared. In the case of contour array stimulation of the human ANF model there is a marked difference in excitation profile widths between non-degenerate and degenerate ANFs and not so for straight array stimulation, while the opposite is true for the GSEF model. These differences cannot be explained in terms of threshold-distance and nerve fibre degeneracy alone, but in terms of the modelled morphology of the ANFs of the two separate models as well. The dendritic part of the Rattay et al. (2001) model, which is assumed myelinated, is reserved in the ANF model and has a diameter half that of the axon (refer to Fig.1). Furthermore, comparison between the internodal lengths of the dendrite and axon shows longer dendritic than axonal internodal lengths. In the GSEF model the dendrite and axonal diameters are the same, and the dendritic internodal lengths are shorter than the axonal internodal lengths. In myelinated fibres located close to electrodes, the threshold current is mainly dependent on the electrode-to-node distances and not so much on the electrode-to-fibre distance as is the case of unmyelinated fibres (refer to Fig. 6 in Rattay, 1987). Furthermore, nerve fibres having a larger diameter are excited at lower threshold currents than thinner fibres (McNeal, 1976). Lastly, the influence of the soma (nerve fibre cell body) must be brought into consideration as well. The soma of the GSEF nerve fibre is 10 µm in diameter and is myelinated, while the human ANF soma is 27 µm in diameter and unmyelinated. In their recently developed human version of the GSEF model, Briaire and Frijns (2005) increased the size of the soma. This change led to upward shifts in threshold compared to their original GSEF model, since the larger soma acted as a current drain.

Black et al. (1980; 1983) measured length constants of 8 – 16 mm (0.54 – 1.09 dB/mm) for monopolar stimulation in vivo in cats. Their three-dimensional resistance model predicts Scala Tympani length constants of 3.04 – 3.57 mm (2.43 – 2.86 dB/mm) in scalar fluids, while the Organ of Corti current length constants are 1.00 – 1.15 mm (7.55 – 8.69 dB/mm). Kral et al. (1998) and Hartmann and Klinke (1990) have reported attenuation slopes of around 3 dB/mm (length constant of about 3 mm) for monopolar stimulation of single fibre units in the basal part of cat cochleae. The length constant value of 2.48 mm predicted with the GSEF model of a guinea-pig ANF was comparable with these length constants for cat. This is in line with a conclusion drawn by Kral et al. (1998) that guinea-pig results by Jolly et al. (1996) compared qualitatively with their cat results. From this it can be inferred that our simple model algorithm can produce reasonable estimates of length constant values.

A recent study of the average forward-masked psychophysical spatial tuning curve slopes obtained for monopolar stimulation of human subjects suggests an average length constant of 6 mm (1.2 dB/mm), which falls within the range of length constants (3 – 16 mm) reported for cat (Nelson et al., 2008). Bingabr et al. (2008) developed an acoustic simulation vocoder model to simulate the effect of excitation spread in the human cochlea. By employing an electrical dynamic range of 15 dB, they calculated excitation spreads (comparable to our ECAP profile widths) of 3.75 – 7.5 mm for a stimulus attenuation length constant of about 2 mm. They attributed the larger length constant value of Nelson et al. (2008) and the large variability across human subjects to possible inaccuracies in the measuring technique employed by Nelson et al., where the tuning curves depend on the survival rate of the subject's ANFs. The length constant value of 1.58 mm predicted with the human ANF model was smaller than the values obtained by Nelson et al. (2008) and Bingabr et al. (2008), although closer to the values of the latter study.

The differences in results between the human ANF model and abovementioned *in vivo* measurements may be due to methodological differences. Our combined volume conduction nerve fibre model made use of single-fibre responses in calculating the neural excitation profiles (Fig. 3) used as input to our simple method, while *in vivo* ECAP measurements in animal and human depends on compound nerve fibre responses. Another way of comparing predicted results with measured psychophysical forward masking experimental results gained from human implantees is modelling the full ECAP method used in NRT. A comprehensive model to predict ECAP data has been developed by Briare and Frijns (2005). However, their results indicated that their human ANF model, which is an adapted version of the GSEF model, could not fully predict measured human ECAP data. Furthermore, the level of physiological detail developed in the GSEF and human ANF models also differs. For instance, in the human ANF model the myelinated internodes were modelled, while not so in the GSEF model. The use of the ANF model in this study in combination with Briare and Frijns' ECAP method could be investigated in a future study to determine whether an improved estimate of ECAP response can thus be accomplished.

In general, ECAP profile widths calculated with the GSEF model (Figs. 5(c) and (d)) were narrower than those calculated with the human ANF model (Figs. 5(a) and (b)). Similar to the ANF model, the ECAP profile widths for both the straight and contour arrays decreased with a decrease in loudness level. The simulated ECAP profile width data were furthermore sensitive to the value of the stimulus attenuation parameter chosen (see Fig. 6 and Table 3). Smaller parameter values predicted smaller ECAP profile widths. Also, a homogeneous, isotropic medium was assumed in the space between the neural and electrode array levels in the simple approximation method. This assumption is in contrast to an actual cochlea, where

the conductivities of the different cochlear tissues vary significantly (see for example Frijns et al., 1995). Since stimulus attenuation is a function of conductivity, predictions of ECAP profile widths will be influenced by a non-homogeneous, anisotropic model of the space between the nerve fibres and the electrode array.

The inclusion of non-homogeneous, anisotropic material properties in the inverse calculation of the ECAP profile widths could also improve the estimated value of the stimulus attenuation parameter and could relate this parameter to the specific location of the electrode array relative to the target nerve fibres. Individualised volume-conduction models that take the location of the electrode array relative to the target nerve fibres of a subject into account, could also improve the stimulus attenuation value estimate.

The observation that stimulus attenuation seemed to vary with stimulus intensity (Table 3) might be related to a more localised spread of excitation at lower stimulus intensities relative to that at higher stimulus intensities. Stimulus decay occurs in two directions: transversal (i.e. perpendicular to the electrode array) and longitudinal (i.e. in a direction parallel to the electrode array) because currents distribute in both directions throughout the cochlear tissue, as reported by Kral et al. (1998). It is possible that the weight that stimulus decay in each direction carries toward the determination of the neural excitation profiles is dependent on stimulus intensity. However, this hypothesis requires further investigation. Variations in cochlear structure and location of the electrode array inside the scala tympani could also lead to variations in the conductivity profile of the cochlear tissue between the array and the nerve fibres and could thus be responsible for observed intersubject variability in stimulus attenuation. A further observation is that the electrode-electrolyte interface impedance is a function of stimulus intensity (i.e., current density through the interface) (Ragheb and

Geddes, 1990). Changes in electrode impedance have been observed *in vivo* and *in vitro* (Newbold et al., 2004; Huang et al., 2007), as well as predicted with a volume-conduction cochlear model (Hanekom, 2005). These changes have been mostly attributed to the growth of fibrous tissue around the electrodes, although Huang et al. (2007) suggested that changes in the perilymph composition after implantation may result in increased impedances. The impedance of the electrode-electrolyte interface is disregarded in the volume-conduction model. In the model a current source is modelled instead of a potential source and the input current will be constant as long as the impedance of the electrode-electrolyte interface stays within required compliance limits. Hence the forward calculation problem does not dependent on the impedance. However, the data from Cohen et al., which are an integral part of the reverse calculation, include the effect of the interface impedance. This may partly explain the dependency of stimulus attenuation on stimulus intensity.

The marked difference in the stimulus attenuation parameter values between the GSEF and human ANF models that best predicted the experimental results of Cohen et al. (2003) can possibly highlight the differences in predictions made between animal and human auditory systems respectively. The differences in cochlear structural morphology between animals and humans, differences in the number and percentage myelination of ANFs and innervation patterns of both inner and outer hair cells across species, may be physiologically significant and care must be taken when extrapolating the animal results to predict results in human implantees (Nadol Jr, 1988; Frijns et al., 2001). Matsuoka et al. (2000) also discussed the differences and similarities between animal and human data. In most animal studies, acutely deafened animals are used. Therefore, a larger relatively intact neural population is expected, in contrast to the more degenerative neural population of the longer-term deafened animal or human. Acutely deafened animal models can thus only give a best case scenario for the

electrical excitation of the human ANF (Abbas and Miller, 2004). In some of the animal experiments, a single electrode is placed inside the cochlea (van den Honert and Stypulkowski, 1984) and in others a multiple-electrode array (Kral et al., 1998), while in humans multiple-electrode arrays are used. The anatomy of the animal and human ANFs also differs (Liberman and Oliver, 1984; Brown, 1987; Nadol Jr, 1988; Nadol Jr et al., 1990; Gleich and Wilson, 1993; Rattay et al., 2001; Briaire and Frijns, 2005). Thus, nerve fibre models based on animal physiology at this stage can only roughly approximate human ANF behaviour.

In spite of a number of shortcomings in the current model as discussed above, results suggested that matching predicted neural excitation profile widths to ECAP data by manipulation of the stimulus attenuation parameter could provide estimates of stimulus attenuation for specific subjects. An accurate estimate of stimulus attenuation could be useful in models that depend on stimulus attenuation to calculate excitation profiles (e.g. Bruce et al., 1999; and Conning, 2006).

CONCLUSION

The human ANF model correctly predicts an increase in excitation spread with an increase in loudness level, as well as wider ECAP profile widths for the straight array compared to those for the contour array. The model also predicts realistic ECAP profile width ranges for the straight array while the lower limit for the width ranges predicted for the contour electrode is comparable to measured width ranges.

Comparison between simulations with the human ANF and GSEF models showed the same trends regarding ECAP profile widths. However, the difference in stimulus attenuation parameter value between the two models that provided the best fit to the measured ECAP width results from the Cohen et al. study, as well as the differences between the neural excitation profiles (Fig. 4) predicted with these models, support the suggestions by Matsuoka et al. (2000) and Briaire and Frijns (2005) that nerve fibre models based on animal physiology at this stage can only roughly approximate human ANF behaviour. It therefore seems that comparison of trends between human ANF behaviour and nerve fibre models forms the extent of usefulness of such models.

It is observed that the fitting of modelled excitation profile widths to measured ECAP profile widths requires different stimulus attenuation values at different stimulation levels. Whether this actually indicates a shortcoming in the model is not certain since the impedance, which is related to stimulus attenuation, could be dependent on stimulus intensity. This observation thus suggests that the effects of stimulus intensity on the mechanisms of stimulus decay and on the electrode-electrolyte interface impedance require further investigation.

ACKNOWLEDGEMENTS

This research has been supported by the National Research Foundation (NRF) of South Africa.

APPENDIX

Equations and parameter values for the human ANF model. An earlier version of the model is described in Smit et al. (2008). A comprehensive description of the development of the model appears in Smit (2008), but a summary is provided here. The model was implemented at body temperature (37°C), but the temperature dependence of the parameters is also stated.

The model was based on the cable model by Rattay (1990; 2001). The dendrite and soma (except for the somal diameter) was still Rattay's model and only the axon was replaced by a recently developed generalised human sensory nerve fibre model, the details of which are presented here. Nodes of Ranvier were unmyelinated active axolemmae with only the axonal nodes utilising the human Ranvier node model described in Smit et al. (Smit et al., 2009). Electrical parameter values for the axonal part of the model are listed in Table A.1. and morphometric parameter values in Table A.2.

The change in the membrane potential (V_k) at the centre of the k^{th} compartment was described by the cable equation (2001)

$$C_{m,k}\frac{d\left(V_k\right)}{dt}=-I_{ion,k}+\frac{\left(V_{k-1}+V_{e,k-1}\right)-\left(V_k+V_{e,k}\right)}{R_{k-1}/2+R_k/2}+\frac{\left(V_{k+1}+V_{e,k+1}\right)-\left(V_k+V_{e,k}\right)}{R_{k+1}/2+R_k/2}. \qquad \text{(A.1)}$$

The membrane potential is given by $V_k = V_{i,k} - V_{e,k} - V_{res}$, having an initial value $V_k(0)$ equal to 0. $V_{i,k}$ is the intracellular potential, $V_{e,k}$ the extracellular potential and V_{res} the resting membrane potential. The HH-model ionic membrane current ($I_{ion,k}$) was described in terms of the transient Na^+ (subscripted '*t*'), persistent Na^+ (subscripted '*p*'), slow K^+ (subscripted '*s*')and leakage ionic membrane currents (Hodgkin and Huxley, 1952)

$$I_{ion}(T) = g_K^{\max}(T) n_s^4 \left(V - V_K(T)\right) + 0.975 g_{Na}^{\max}(T) m_t^3 h\left(V - V_{Na}(T)\right) + 0.025 g_{Na}^{\max}(T) m_p^3 h\left(V - V_{Na}(T)\right) + g_L(T)\left(V - V_L(T)\right) \quad \left[mA/cm^2\right] \tag{A.2}$$

Equilibrium potentials were given by

$$V_{Na}, V_K, V_L = \frac{1000 R T_K}{F} \ln\left(\frac{[ion]_o}{[ion]_i}\right) - V_{res} \quad [mV] \tag{A.3}$$

with R the universal gas constant, F the Faraday constant, T_K the temperature (in Kelvin) and $[ion]_o/[ion]_i$ the extracellular to intracellular ion concentration ratio for Na^+, K^+ and leakage ions respectively.

Myelinated internodes were simple double cable structures (Blight, 1985). The leaky myelin sheath and axolemma was considered combined together in series, having a high resistance and low capacitance. The total capacitance was given by

$$c_{m,k} = \left(\frac{1}{c_{mem}} + \frac{N_{my}}{c_{my}}\right)^{-1} \quad \left[\mu F/cm^2\right] \tag{A.4}$$

with c_{mem} the same value as the nodal membrane capacitance and c_{my} the myelin membrane capacitance (Table A.1.). The number of myelin layers (N_{my}) was given by

$$N_{my} = \left\lfloor 0.5\left(d_f - d_a\right)\right\rfloor / l_{my}, \tag{A.5}$$

with d_f the total internodal nerve fibre diameter (cm), d_a the internodal axolemmal diameter (cm) and l_{my} the myelin layer thickness equal to 0.016 μm (1985).

The internodal conductance was given by

$$g_{\text{int}}(T) = \frac{1}{\left(N_{my} R_{my}(T)\right) + R_{mem}(T)} \quad \left[mS/cm^2\right] \tag{A.6}$$

with N_{my} number of myelin layers, R_{my} the temperature-dependent myelin membrane resistance and R_{mem} the temperature-dependent axolemmal membrane resistance (Table A.2 and Blight (1985)). I_{int} was therefore given by

$$I_{ion,k}(T) = I_{\text{int}}(T) = g_{\text{int}}(T)V \qquad \left[\mu A/cm^2\right]. \tag{A.7}$$

---------- *Suggested position of Table A.1.* ----------

---------- *Suggested position of Table A.2.* ----------

The dynamics of the opening probabilities (m_t, m_p, h and n_s respectively) of the ion channels were described by

$$\frac{dx}{dt} = a_x(V)\left[1-x\right] - b_x(V)\,x, \;\; x = m_t, m_p, n_s, h \tag{A.8}$$

with initial values (Hodgkin and Huxley, 1952)

$m_p(0) = m_t(0) = 0.05$

$h(0) = 0.6$

$n_s(0) = 0.32$

Ion channel gating variables were given by

$$\alpha_{mt}, \alpha_{ns} = AQ_{10}^{(T-T_0)/10} \cdot \frac{B - CV}{D\left(\exp\left(B - CV\right)\right) - 1} \qquad [m/s], \tag{A.9a}$$

$$\beta_{mt}, \beta_{ns}, \alpha_h = AQ_{10}^{(T-T_0)/10} \cdot B \exp\left(\frac{-V}{C}\right) \qquad [m/s], \tag{A.9b}$$

$$\beta_h = AQ_{10}^{(T-T_0)/10} \cdot \frac{1}{1 + \exp\left(B - CV\right)}, \qquad [m/s] \tag{A.9c}$$

$$\alpha_{mp} = AQ_{10}^{(T-T_0)/10} \cdot \frac{B - C\left(V - \Delta V\right)}{D\left(\exp\left(B - C\left(V - \Delta V\right)\right)\right) - 1} \qquad [m/s], \tag{A.9d}$$

$$\beta_{mp} = AQ_{10}^{(T-T_0)/10} \cdot B \exp\left(\frac{-\left(V - \Delta V\right)}{C}\right) \qquad [m/s], \tag{A.9e}$$

where ΔV indicates that the persistent sodium current activated 20 mV more negative than the transient sodium current. Acceleration of the activation and inactivation of the membrane's permeability to specific ion species, as suggested by Huxley (1959), are given by parameter *A* values (Table A.3). Parameter *B*, *C* and *D* the original HH model parameters (Hodgkin and Huxley, 1952) (Table A.3).

---------- *Suggested position of Table A.3.* ----------

REFERENCES

Abbas PJ, Brown CJ, Shallop JK, Firszt JB, Hughes ML, Hong SH, Staller SJ. Summary of results using the Nucleus CI24M implant to record the electrically evoked compound action potential. Ear Hear, 1999; 20: 45-59.

Abbas PJ, Hughes ML, Brown CJ, Miller CA, South H. Channel interaction in cochlear implant users evaluated using the electrically evoked compound action potential. Audiol Neurootol, 2004; 9: 203-13.

Abbas PJ, Miller CA. Biophysics and physiology. In Zeng F-G, Popper AN, Fay RR, editors. Cochlear Implants: Auditory prostheses and electric hearing. Springer-Verlag: New York, 2004; 149-212.

Arts HA, Jones DA, Anderson DJ. Prosthetic stimulation of the auditory system with intraneural electrodes. Ann Otol Rhinol Laryngol Suppl, 2003; 191: 20-5.

Atkins PW. Physical Chemistry, Fifth ed. Oxford University Press: Oxford, 1995.

Bingabr M, Espinoza-Varas B, Loizou PC. Simulating the effect of spread of excitation in cochlear implants. Hear Res, 2008; 241: 73-9.

Black RC, Clark GM. Differential electrical excitation of the auditory nerve. J Acoust Soc Am, 1980; 67: 868-74.

Black RC, Clark GM, Tong YC, Patrick JF. Current distributions in cochlear stimulation. Ann N Y Acad Sci, 1983; 405: 137-45.

Blight AR. Computer simulation of action potentials and afterpotentials in mammalian myelinated axons: The case for a lower resistance myelin sheath. Neuroscience, 1985; 15: 13-31.

Briaire JJ, Frijns JHM. Unraveling the electrically evoked compound action potential. Hear Res, 2005; 205: 143-56.

Briaire JJ, Frijns JHM. The consequences of neural degeneration regarding optimal cochlear implant position in scala tympani: A model approach. Hear Res, 2006; 214: 17-27.

Brown MC. Morphology of labeled afferent fibers in the guinea pig cochlea. J Comp Neurol, 1987; 260: 591-604.

Bruce IC, White MW, Irlicht LS, O'Leary SJ, Dynes S, Javel E, Clark GM. A stochastic model of the electrically stimulated auditory nerve: single-pulse response. IEEE Trans Biomed Eng, 1999; 46: 617-29.

Chatterjee M, Shannon RV. Forward masked excitation patterns in multielectrode electrical stimulation. J Acoust Soc Am, 1998; 103: 2565-72.

Cohen LT, Richardson LM, Saunders E, Cowan RSC. Spatial spread of neural excitation in cochlear implant recipients: comparison of improved ECAP method and psychophysical forward masking. Hear Res, 2003; 179: 72-87.

Cohen LT, Saunders E, Clark GM. Psychophysics of a prototype peri-modiolar cochlear implant electrode array. Hear Res, 2001; 155: 63-81.

Conning M. Acoustic modelling of cochlear implants. MIng dissertation. University of Pretoria, Pretoria, South Africa, 2006: 1-171.

Dillier N, Lai WK, Almqvist B, Frohne C, Müller-Deile J, Stecker M, van Wallenberg E. Measurement of the electrically evoked compound action potential via a neural response telemetry system. Ann Otol Rhinol Laryngol, 2002; 111: 407-14.

Fayad JN, Linthicum Jr FH. Multichannel cochlear implants: Relation of histopathology to performance. Laryngoscope, 2006; 116: 1310-20.

Franck KH, Norton SJ. Estimation of psychophysical levels using the electrically evoked compound action potential measured with the neural response telemetry capabilities of Cochlear Corporation's CI24M device. Ear Hear, 2001; 22: 289-99.

Frijns JHM, Briaire JJ, Grote JJ. The importance of human cochlear anatomy for the results of modiolus-hugging multichannel cochlear implants. Otol Neurotol, 2001; 22: 340-9.

Frijns JHM, Briaire JJ, Schoonhoven R. Integrated use of volume conduction and neural models to simulate the response to cochlear implants. Simpra, 2000; 8: 75-97.

Frijns JHM, de Snoo SL, Schoonhoven R. Potential distributions and neural excitation patterns in a rotationally symmetric model of the electrically stimulated cochlea. Hear Res, 1995; 87: 170-86.

Frijns JHM, de Snoo SL, ten Kate JH. Spatial selectivity in a rotationally symmetric model of the electrically stimulated cochlea. Hear Res, 1996; 95: 33-48.

Frijns JHM, ten Kate JH. A model of myelinated nerve fibres for electrical prosthesis design. Med Biol Eng Comput, 1994; 32: 391-8.

Gleich O, Wilson S. The diameters of guinea pig auditory nerve fibres: distribution and correlation with spontaneous rate. Hear Res, 1993; 71: 69-79.

Glueckert R, Pfaller K, Kinnefors A, Rask-Andersen H, Schrott-Fischer A. The human spiral ganglion: New insights into ultrastructure, survival rate and implications for cochlear implants. Audiol Neurotol, 2005; 10: 258-73.

Hanekom T. Modelling encapsulation tissue around cochlear implant electrodes. Med Biol Eng Comput, 2005; 43: 47-55.

Hanekom T. Three-dimensional spiraling finite element model of the electrically stimulated cochlea. Ear Hear, 2001; 22: 300-15.

Hartmann R, Klinke R. Inpulse patterns of auditory nerve fibres to extra and intracochlear electrical stimulation. Acta Oto-Laryngologica, 1990; 469: 128-34.

Hille B. Ionic Channels of Excitable Membrane, Third ed. Sinauer Associates Inc.: Sunderland, Massachusetts, 2001: 1-814.

Hodgkin AL, Huxley AF. A quantitative description of membrane current and its application to conduction and excitation in nerve. J Physiol (Lond), 1952; 117: 500-44.

Huang CQ, Tykocinski M, Stathopoulos D, Cowan RSC. Effects of steroids and lubricants on electrical impedance and tissue response following cochlear implantation. Cochlear Implants International, 2007; 8: 123-47.

Huxley AF. Ion movements during nerve activity. Ann N Y Acad Sci, 1959; 81: 221-46.

Javel E, Tong YC, Shepherd RK, Clark GM. Responses of cat auditory nerve fibers to biphasic electrical current pulses. Ann Otol Rhinol Laryngol, 1987; 96: 26-30.

Jolly CN, Spelman FA, Clopton BM. Quadrupolar stimulation for cochlear prostheses: Modeling and experimental data. IEEE Trans Biomed Eng, 1996; 43: 857-65.

Kral A, Hartmann R, Mortazavi D, Klinke R. Spatial resolution of cochlear implants: The electrical field and excitation of auditory afferents. Hear Res, 1998; 121: 11-28.

Kwon BJ, van den Honert C. Effect of electrode configuration on psychophysical forward masking in cochlear implant listeners. J Acoust Soc Am, 2006; 119: 2994-3002.

Leake PA, Rebscher SJ. Anatomical considerations of electrical stimulation. In Zeng F-G, Popper AN, Fay RR, editors. Cochlear Implants: Auditory prostheses and electric hearing. Springer-Verlag: New York, 2004; 101-48.

Liberman MC, Oliver ME. Morphometry of intracellularly labeled neurons of the auditory-nerve: correlations with functional properties. J Comp Neurol, 1984; 223: 163-76.

Matsuoka AJ, Abbas PJ, Rubinstein JT, Miller CA. The neuronal response to electrical constant-amplitude pulse train stimulation: evoked compound action potential recordings. Hear Res, 2000; 149: 115-28.

McNeal DR. Anaysis of a model for excitation of myelinated nerve. IEEE Trans Biomed Eng, 1976; 23: 329-37.

Middlebrooks JC, Snyder RL. Auditory prosthesis with a penetrating nerve array. J Assoc Res Otolaryngol, 2007; 8: 258-79.

Middlebrooks JC, Snyder RL. Intraneural stimulation for auditory prosthesis: Modiolar trunk and intracranial stimulation sites. Hear Res, 2008; 242: 52-63.

Miller CA, Abbas PJ, Brown CJ. Electrically evoked auditory brainstem response to stimulation of different sites in the cochlea. Hear Res, 1993; 66: 130-42.

Miller CA, Abbas PJ, Hay-McCutcheon MJ, Robinson BK, Nourski KV, Jeng F-C. Intracochlear and extracochlear ECAP's suggest antidromic action potentials. Hear Res, 2004; 198: 75-86.

Miller CA, Abbas PJ, Nourski KV, Hu N, Robinson BK. Electrode configuration influences action potential initiation site and ensemble stochastic response properties. Hear Res, 2003; 175: 200-14.

Miller CA, Abbas PJ, Rubinstein JT. An empirically based model of the electrically evoked compound action potential. Hear Res, 1999; 135: 1-18.

Nadol Jr JB. Patterns of neural degeneration in the human cochlea and auditory nerve: implications for cochlear implantation. Otolaryngol Head Neck Surg, 1997; 117: 220-8.

Nadol Jr JB. Comparative anatomy of the cochlea and auditory nerve in mammals. Hear Res, 1988; 34: 253-66.

Nadol Jr JB, Burgess BJ, Reisser C. Morphometric analysis of normal human spiral ganglion cells. Ann Otol Rhinol Laryngol, 1990; 99: 340-8.

Nadol Jr JB. Degeneration of cochlear neurons as seen in the spiral ganglion of man. Hear Res, 1990; 49: 141-54.

Nelson DA, Donaldson GS, Kreft H. Forward-masked spatial tuning curves in cochlear implant users. J Acoust Soc Am, 2008; 123: 1522-43.

Newbold C, Richardson R, Huang CQ, Milojevic D, Cowan RSC, Shepherd RK. An in vitro model for investigating impedance changes with cell growth and electrical stimulation: Implications for cochlear implants. J Neural Eng, 2004; 1: 218-27.

Niparko JK. Cochlear implants: Clinical applications. In Zeng F-G, Popper AN, Fay RR, editors. Cochlear Implants: Auditory prostheses and electric hearing. Springer-Verlag: New York, 2004; 53-100.

O'Leary SJ, Black RC, Clark GM. Current distributions in the cat cochlea: A modelling and electrophysiological study. Hear Res, 1985; 18: 273-81.

Ragheb T, Geddes LA. Electrical properties of metallic electrodes. Med Biol Eng Comput, 1990; 28: 182-6.

Ranck Jr JB. Which elements are excited in electrical stimulation of mammalian central nervous system: a review. Brain Res, 1975; 98: 417-40.

Rattay F. Ways to approximate current-distance relations for electrically stimulated fibers. J Theor Biol, 1987; 125: 339-49.

Rattay F. Electrical nerve stimulation: theory, experiments and applications. Springer Verlag: Wien New York, 1990: 1-264.

Rattay F, Lutter P, Felix H. A model of the electrically excited human cochlear neuron I. Contribution of neural substructures to the generation and propagation of spikes. Hear Res, 2001; 153: 43-63.

Rebscher SJ, Snyder RL, Leake PA. The effect of electrode configuration and duration of deafness on threshold and selectivity of responses to intracochlear electrical stimulation. J Acoust Soc Am, 2001; 109: 2035-48.

Reid G, Bostock H, Schwarz JR. Quantitative description of action potentials and membrane currents in human node of Ranvier. J Physiol (Lond), 1993; 467: 247P.

Reid G, Scholz A, Bostock H, Vogel W. Human axons contain at least five types of voltage-dependent potassium channel. J Physiol (Lond), 1999; 518: 681-96.

Rosbe KW, Burgess BJ, Glynn RJ, Nadol Jr JB (1996) Morphologic evidence for three cell types in the human spiral ganglion. Hear Res 93:120-127

Scholz A, Reid G, Vogel W, Bostock H. Ion channels in human axons. J Neurophysiol, 1993; 70: 1274-9.

Schuknecht HF. Pathology of the ear, 2nd ed. Lea and Febiger: Philadelphia, 1993.

Schwarz JR, Eikhof G. Na currents and action potentials in rat myelinated nerve fibres at 20 and 37 °C. Pflügers Arch, 1987; 409: 569-77.

Schwarz JR, Reid G, Bostock H. Action potentials and membrane currents in the human node of Ranvier. Pflügers Arch - Eur J Physiol, 1995; 430: 283-92.

Shannon RV, Fu Q-J, Galvin III JJ, Friesen L. Speech perception with cochlear implants. In Zeng F-G, Popper AN, Fay RR, editors. Cochlear Implants: Auditory prostheses and electric hearing. Springer-Verlag: New York, 2004; 334-76.

Shepherd RK, Hatshushika S, Clark GM. Electrical stimulation of the auditory nerve: The effect of electrode position on neural excitation. Hear Res, 1993; 66: 108-20.

Smit JE. Modelled response of the electrically stimulated human auditory nerve fibre. Ph.D. thesis. University of Pretoria, Pretoria, 2008:

Smit JE, Hanekom T, Hanekom JJ. Predicting action potential characteristics of human auditory nerve fibres through modification of the Hodgkin-Huxley equations. S Afr J Sci, 2008; 104: 284-92.

Smit JE, Hanekom T, Hanekom JJ. Modelled temperature-dependent excitability behaviour of a single Ranvier node for a human peripheral sensory nerve fibre. Biol Cybern, 2009; 100: 49-58.

Spelman FA, Clopton BM, Pfingst BE. Tissue impedance and current flow in the implanted ear. Implications for the cochlear prosthesis. Ann Otol Rhinol Laryngol Suppl, 1982; 98: 3-8.

Spoendlin H, Schrott A. Analysis of the human auditory nerve. Hear Res, 1989; 43: 25-38.

Townshend B, White RL. Reduction of electrical interaction in auditory prostheses. IEEE Trans Biomed Eng, 1987; 34: 891-7.

van den Honert C, Stypulkowski PH. Physiological properties of the electrically stimulated auditory nerve. II. Single fiber recordings. Hear Res, 1984; 14: 225-43.

van den Honert C, Stypulkowski PH. Single fiber mapping of spatial excitation patterns in the electrically stimulated auditory nerve. Hear Res, 1987; 29: 195-206.

van der Heijden M, Kohlrausch A. Using an excitation-pattern model to predict auditory masking. Hear Res, 1994; 80: 38-52.

van Wieringen A, Carlyon RP, Laneau J, Wouters J. Effects of waveform shape on human sensitivity to electrical stimulation of the inner ear. Hear Res, 2005; 200: 73-86.

Vanpoucke FJ, Zarowski AJ, Peeters SA. Identification of the impedance model of an implanted cochlear prosthesis from intracochlear potential measurements. IEEE Trans Biomed Eng, 2004; 51: 2174-83.

Wesselink WA, Holsheimer J, Boom HBK (1999) A model of the electrical behaviour of myelinated sensory nerve fibres based on human data. Med Biol Eng Comput 37:228-235

Zimmermann CE, Burgess BJ, Nadol Jr JB. Patterns of degeneration in the human cochlear nerve. Hear Res, 1995; 90: 192-201.

Figure captions

Fig. 1. The two-dimensional finite element model geometry of a plane through the cochlea. The medial and lateral positions of the electrode array are shown as circular geometries towards the top of the scala tympani. The labels $\boldsymbol{n_1}$ to $\boldsymbol{n_{12}}$ indicate the twelve locations (nodes) in the neural tissue where electrical potential values are calculated. (Figure used with permission from Hanekom (2001))

Fig. 2. Representation of the human auditory nerve fibre. The dendrite and axon are divided into cylindrical compartments, while the soma is assumed to be spherical (Rattay et al., 2001). The dendrite is considered myelinated, with five internodes of variable lengths (Rattay et al., 2001). The myelin of these internodes is assumed a perfect insulator. The presomatic segment is divided into three sections (not indicated on sketch). Although the soma employs the Hodgkin-Huxley dynamics as described by Rattay et al. (2001), its diameter is smaller than in the Rattay model. The axonal section employs the human sensory nerve fibre dynamics and morphometry and morphology. Unlike in the Rattay model, internodal lengths are considered constant and are shorter than in the Rattay model.

Fig. 3. Outline of the simple method used to estimate ECAP profile widths at the electrode array level for non-degenerate and degenerate nerve fibres. Representations of the (a) volume conductance cochlear model and (b) nerve fibre model. (c) The output of the ANF model is a neural excitation profile indicating the threshold currents at which the nerve fibres along the basilar membrane become excited. (d) Neural excitation spread is estimated at the neural level and (e) the simple method estimates ECAP profile widths at the electrode array level.

Fig. 4. (a, b) Neural excitation profiles calculated with the volume-conduction ANF model (open markers). Predicted neural excitation profile widths for 80%, 50% and 20% loudness levels for Cohen et al.'s (2003) subjects S3 (straight array, solid lines) and C1 (contour array, dot-dash lines) for (a) a degenerate and (b) a non-degenerate ANF population are indicated with horizontal lines. (c, d) Neural excitation profiles simulated with the GSEF model combined with the volume-conduction model. All conditions are the same as in (a) and (b).

Fig. 5. Normalised ECAP profile width ranges, at the electrode array level, calculated with the ANF model for 80%, 50% and 20% loudness levels for (a) straight array and (b) contour array for a degenerate and non-degenerate ANF population. Calculations are for a stimulus attenuation length constant of 1.58 mm. Filled symbols indicates degenerate and open symbols non-degenerate ANF cases respectively. The horizontal line indicates the predicted widths. (c, d) Normalised ECAP profile width ranges calculated with the GSEF model. ECAP profile widths shown are for a stimulus attenuation length constant of 2.48 mm. All conditions are the same as in (a) and (b).

Fig. 6. Predicted ECAP profile widths, at the electrode array level, for 80%, 50% and 20% loudness levels for subject S3 (straight array) for (a) a degenerate and (b) a non-degenerate ANF population. The ECAP profile widths are plotted against stimulus attenuation length constant.

Table 1. Measured ECAP profile width ranges for electrode 6 (Cohen et al., 2003) for four straight array and three contour array subjects. Width data at the 20% level were available for only one subject using the straight array, and for none of the subjects using the contour array. Profile widths were measured at FWHM, i.e. the profile width at 50% of the peak amplitude.

	80% loudness level	**50% loudness level**	**20% loudness level**
Straight array	4.26 mm to 6.78 mm	4.58 mm to 6.67 mm	3.73 mm (measured for single subject)
Contour array	2.98 mm to 3.41 mm	2.13 mm to 3.62 mm	No data available

Table 2. Simulated ECAP profile widths at the electrode array level for a stimulation attenuation length constant of 1.58 mm. Similar to Cohen et al. (2003) profile widths were measured at FWHM, i.e. the profile width at 50% of the peak amplitude.

	80% loudness level	**50% loudness level**	**20% loudness level**
Straight array: degenerate	3.88 mm to 6.76 mm	3.88 mm to 5.86 mm	3.65 mm to 5.29 mm
Contour array: degenerate	3.67 mm to 3.82 mm	3.31 mm to 3.67 mm	3.15 mm
Straight array: non-degenerate	3.48 mm to 6.64 mm	3.48 mm to 5.39 mm	2.92 mm to 5.09 mm
Contour array: non-degenerate	3.44 mm to 3.57 mm	3.21 mm to 3.44 mm	3.02 mm

Table 3: Stimulus attenuation length constant values that provide the best fit of the modelled data to the data of Cohen et al. (2003).

	80% loudness level	**50% loudness level**	**20% loudness level**
Straight array: degenerate	1.45 – 3.47 mm	1.45 – 3.47 mm	1.45 – 1.58 mm
Contour array: degenerate	1.45 – 1.58 mm	1.45 – 1.74 mm	No data to compare with
Straight array: non-degenerate	1.45 – 3.47 mm	1.45 – 3.47 mm	1.93 – 2.17 mm
Contour array: non-degenerate	1.45 – 1.58 mm	1.45 – 1.74 mm	No data to compare with

Table A.1. Electrical parameters for the axonal part of the human auditory nerve fibre model.

Parameter	Value	Q_{10}	T_0 (°C)	Reference
Membrane resting potential (V_{rest})	-79.4 mV	1.0356 for all T ≤ 20°C 1.0345 for all T > 20°C	6.3	(Hodgkin and Huxley, 1952; Schwarz et al., 1995; Wesselink et al., 1999) †
Gas constant (R)	8.3145 J/K.mol			(Atkins, 1995)
Faraday constant (F)	9.6485×10^4 C/mol			(Atkins, 1995)
$[Na^+]_o/[Na^+]_i$	7.2102			(Hodgkin and Huxley, 1952; Schwarz et al., 1995; Wesselink et al., 1999; Hille, 2001) #
$[K^+]_o/[K^+]_i$	0.0361			(Reid et al., 1993; Scholz et al., 1993; Schwarz et al., 1995; Reid et al., 1999)
$[Leakage]_o/[Leakage]_i$	0.036645			(Scholz et al., 1993; Schwarz et al., 1995) ††
Sodium conductance (g_{Na})	640.00 mS/cm^2	1.02	24	(Scholz et al., 1993; Hille, 2001)
Potassium conductance (g_K)	60.0 mS/cm^2	1.16	20	(Reid et al., 1993; Scholz et al., 1993; Schwarz et al., 1995; Reid et al., 1999) ††
Leakage conductance (g_L)	57.5 mS/cm^2	1.418	24	(Schwarz and Eikhof, 1987; Scholz et al., 1993; Schwarz et al., 1995) ††
Axoplasmic (intracellular) resistivity (ρ_{ax})	0.025 kΩ.cm	$(1.35)^{-1}$	37	(Wesselink et al., 1999) †
Membrane capacitance (c_{mem})	2.8 µF/cm^2			(Schwarz et al., 1995) *
Myelin membrane capacitance (c_{my})	0.6 µF/cm^2			(Blight, 1985)
Membrane resistance (R_{mem})	4.8707×10^4 Ω.cm^2	$(1.3)^{-1}$	25	(Blight, 1985) †
Myelin membrane resistance (R_{my})	104 Ω.cm^2	$(1.3)^{-1}$	25	(Blight, 1985) †

† Value deduced from reference(s) and then optimised for model. Q_{10} value not from reference, but optimised for model

Discrepancy exists between HH model value and values for human. Value hence optimised for model

†† Values deduced from reference(s) and corrected for concentration and temperature differences

* Considered constant for temperatures between 20 and 42°C

Table A.2. Model morphometric parameters.

Parameter	Value	Reference
Fibre diameter	3.75 µm	(Rosbe et al., 1996)
Internodal axon diameter	2.63 µm	*
Myelin layer thickness	0.016 µm	(Blight, 1985)
Number of myelin layers (N_{my})	35	*
Internodal length (L_{int})	77.4 µm	(Wesselink et al., 1999)
Nodal diameter	1.23 µm	*
Nodal length	1.061 µm	*
Dendrite diameter	1.0 µm	(Rattay et al., 2001)
Soma diameter	27.0 µm	(Schuknecht, 1993; Rosbe et al., 1996)

* Deduced from previous parameters

Table A.3. Parameters used for calculation of the voltage-dependent opening and closing rates of the ion channels for the axonal part of the human auditory nerve fibre model. The transient sodium current activation parameters are subscripted with a '*t*' and the persistent sodium current activation parameters by a '*p*'.

Parameter	Q_{10}	T_0 (°C)	A	B	C	D
α_{mt}	2.16	20	4.42	2.5	0.1	1
β_{mt}	2.16	20	4.42	4.0	18	-
α_h	1.5	20	1.47	0.07	20	-
β_h	1.5	20	1.47	3.0	0.1	-
α_{ns}	1.5	20	0.2	1.0	0.1	10
β_{ns}	1.5	20	0.2	0.125	80	-
α_{mp}	1.99	20	2.06	2.5	0.1	1
β_{mp}	1.99	20	2.06	4.0	18	-

Fig. 1

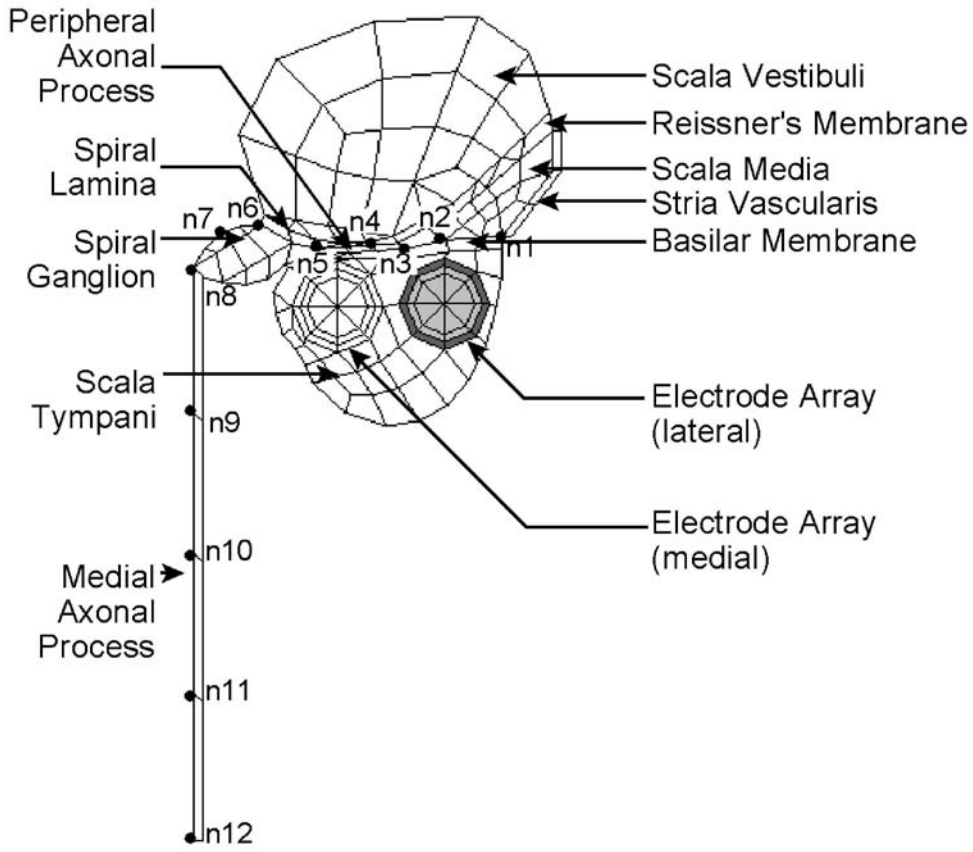
Peripheral
Axonal
Process
Spiral
Lamina
Spiral
Ganglion
Scala
Tympani
Medial
Axonal
Process
n1
n2
n3
n4
n5
n6
n7
n8
n9
n10
n11
n12
Scala Vestibuli
Reissner's Membrane
Scala Media
Stria Vascularis
Basilar Membrane
Electrode Array
(lateral)
Electrode Array
(medial)

Fig. 2

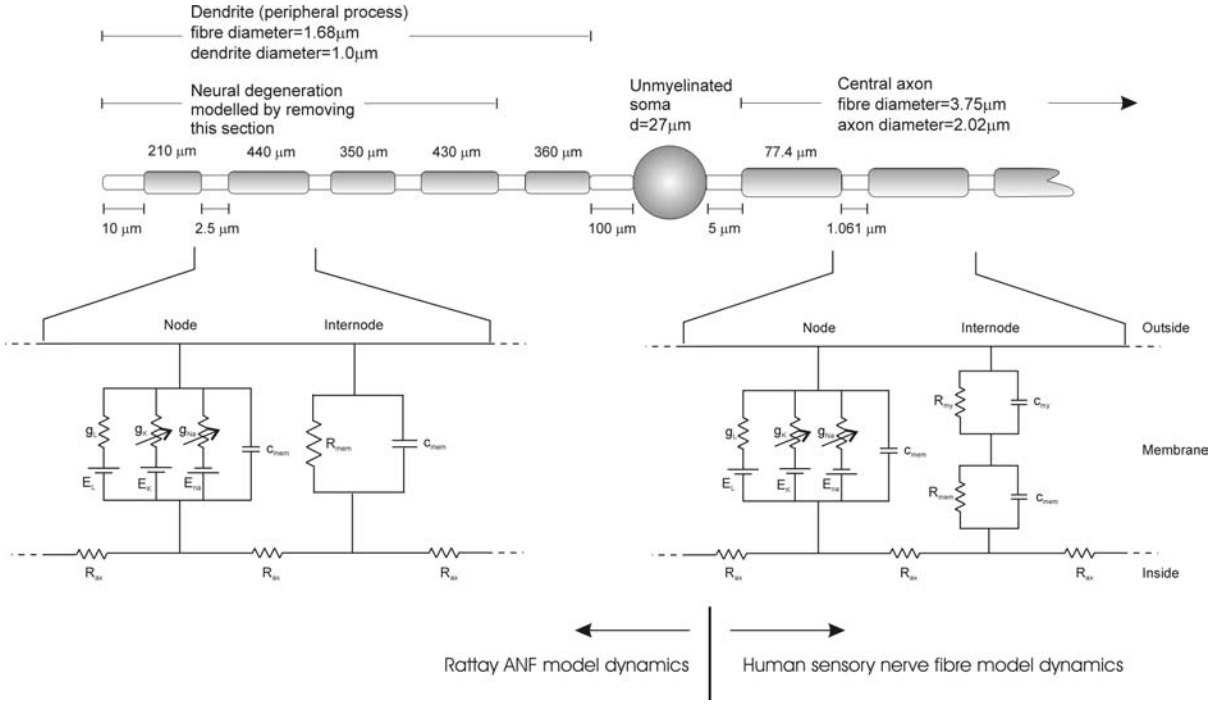
Dendrite (peripheral process)
fibre diameter=1.68μm
dendrite diameter=1.0μm
Neural degeneration
modelled by removing
this section
Unmyelinated
soma
d=27μm
Central axon
fibre diameter=3.75μm
axon diameter=2.02μm
210 μm
440 μm
350 μm
430 μm
360 μm
77.4 μm
10 μm
2.5 μm
100 μm
5 μm
1.061 μm
Node
Internode
Node
Internode
Outside
Membrane
Inside
Rattay ANF model dynamics
Human sensory nerve fibre model dynamics

Fig. 3

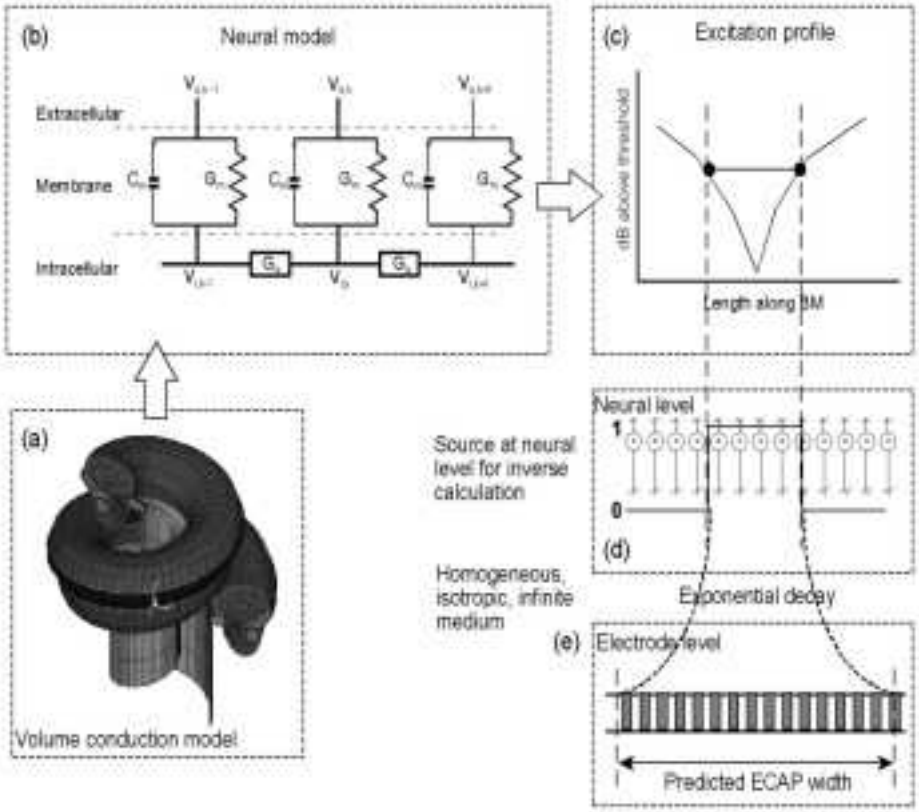
(b)
Neural model
Extracellular
Membrane
Intracellular
(c)
Excitation profile
dB above threshold
Length along BM
(a)
Volume conduction model
Source at neural level for inverse calculation
Neural level
1
0
(d)
Homogeneous, isotropic, infinite medium
Exponential decay
(e)
Electrode level
Predicted ECAP width

Fig. 4

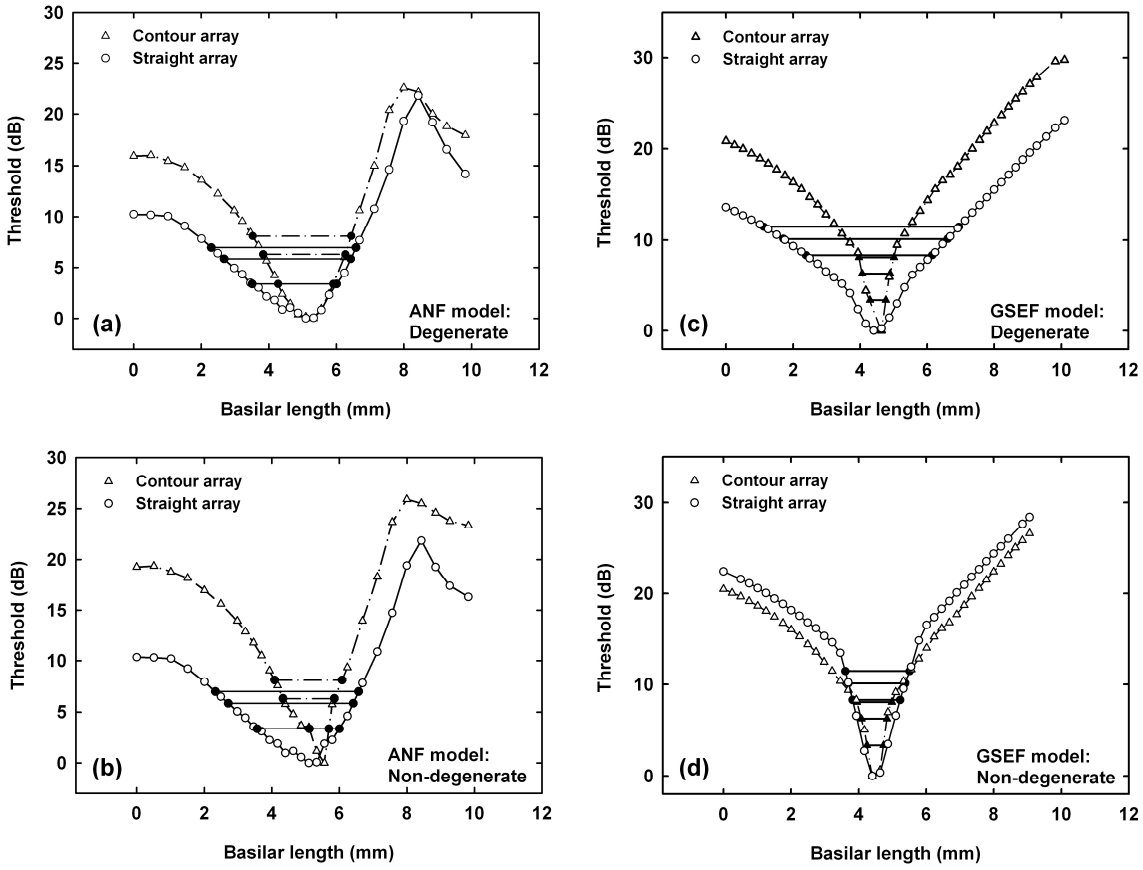
Contour array
Straight array
Threshold (dB)
Basilar length (mm)
(a)
ANF model:
Degenerate
(b)
ANF model:
Non-degenerate
(c)
GSEF model:
Degenerate
(d)
GSEF model:
Non-degenerate

Fig. 5

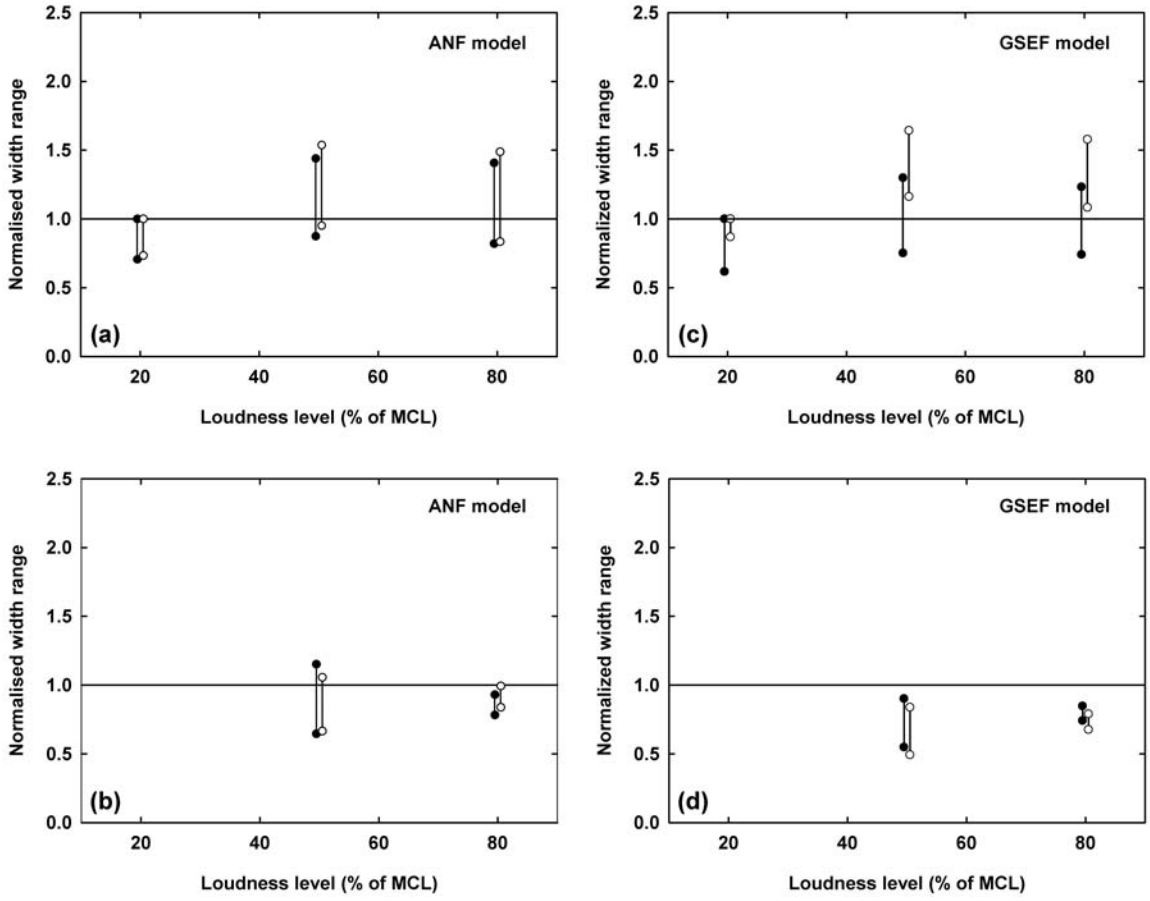
ANF model
GSEF model
Normalised width range
Normalized width range
Loudness level (% of MCL)
(a)
(b)
(c)
(d)
0.0
0.5
1.0
1.5
2.0
2.5
20
40
60
80

Fig. 6

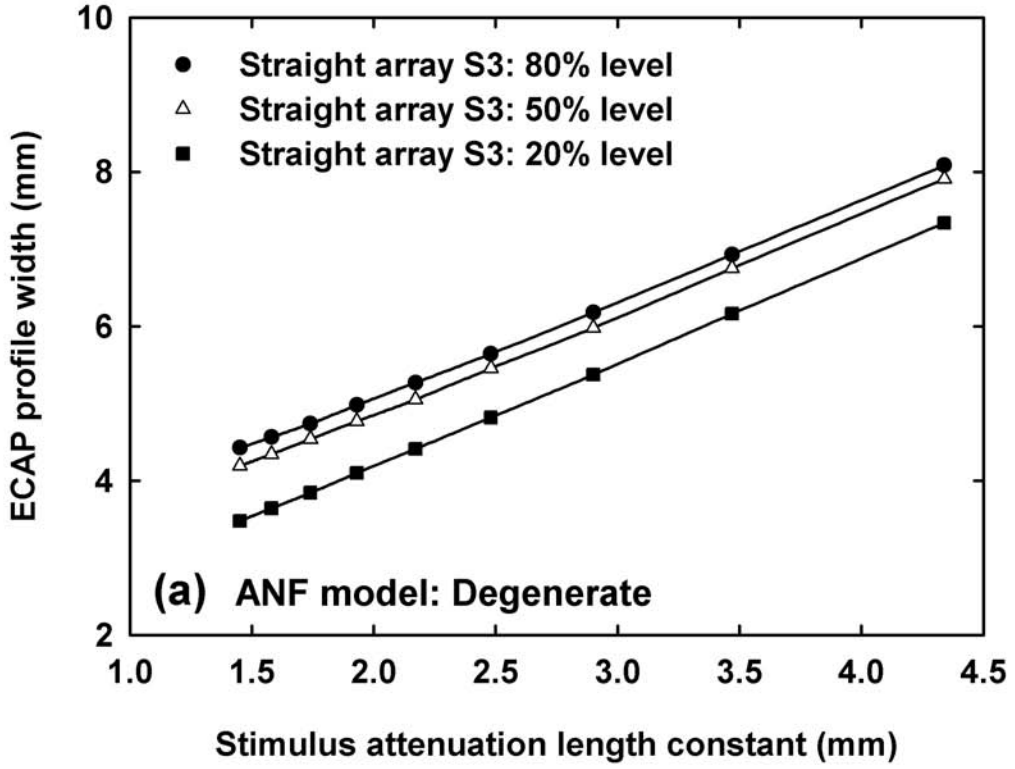
Straight array S3: 80% level
Straight array S3: 50% level
Straight array S3: 20% level
(a) ANF model: Degenerate
ECAP profile width (mm)
Stimulus attenuation length constant (mm)
10
8
6
4
2
1.0
1.5
2.0
2.5
3.0
3.5
4.0
4.5

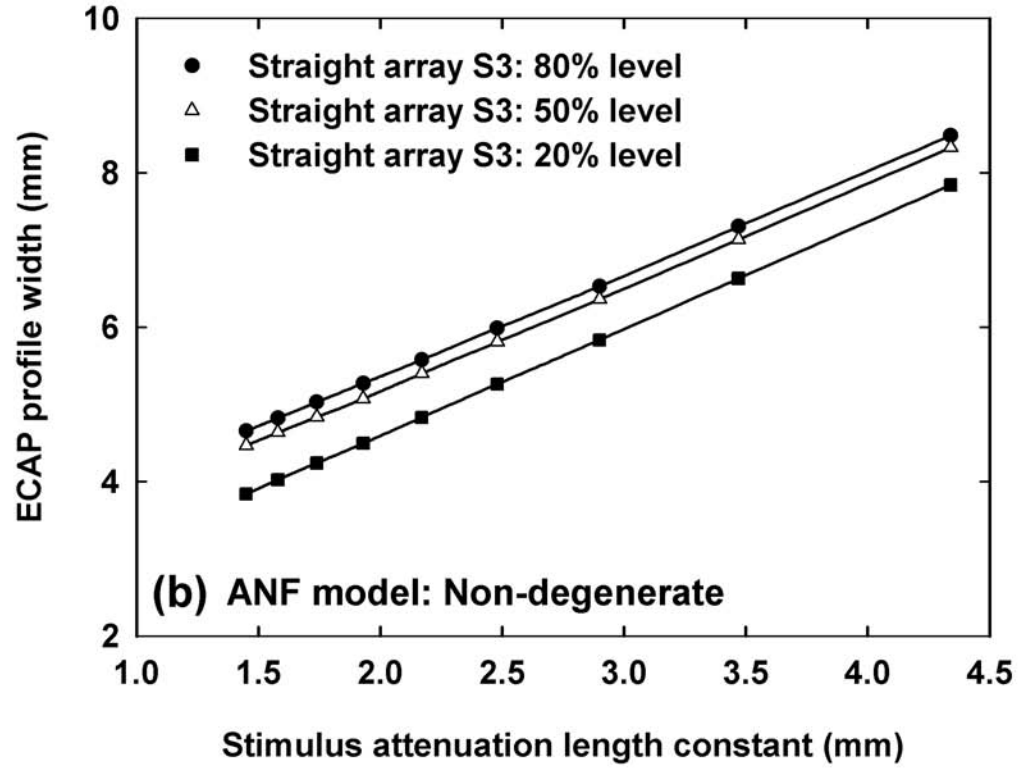
Straight array S3: 80% level
Straight array S3: 50% level
Straight array S3: 20% level
(b) ANF model: Non-degenerate
ECAP profile width (mm)
Stimulus attenuation length constant (mm)
10
8
6
4
2
1.0
1.5
2.0
2.5
3.0
3.5
4.0
4.5